

## ***Interactive comment on “Failure criteria for porous dome rocks and lavas: a study of Mt. Unzen, Japan” by Rebecca Coats et al.***

**Rebecca Coats et al.**

r.coats@liverpool.ac.uk

Received and published: 31 July 2018

Lines 39-56: Sparks (1997) is highly relevant to this study, and is a surprising omission here. Sparks (1997) The causes and consequences of pressurisation in lavas dome eruptions. Earth and Planetary Science Letters 150(3-4): 177-189 - We thank the reviewer for bringing this to our attention and have added the reference in question, an oversight given its relevance to the fundamentals of this study.

Line 66: how do the authors define the "temperature range of interest"? - Webb and Dingwell (1989) compiled a large dataset of elastic modulus at infinite frequency,  $G_{\infty}$ , for silicate melts and many other compounds, over a range of temperatures. Previous studies found that  $G_{\infty}$  ranges from 5 to 42 GPa at room temperature for glasses

Printer-friendly version

Discussion paper



with silica contents ranging between 5-99 mole% (Bansal and Doremus, 1986), and at temperatures between 400 and 1600 °C,  $G_{\infty} = 33 \text{ GPa} \pm 5\%$  (Bucaro and Dardy, 1974). Webb and Dingwell (1989) added data to find that for silicate melts and glasses,  $G_{\infty}$  ranges between 3.2 and 32 GPa and thus can be approximated at  $1010 \pm 0.5$  as it only weakly varies with temperature (unlike viscosity). This brings an important simplification to the modeling of viscoelastic melts, which has been pivotal in its integration to volcanology. Therefore, we can assume  $G_{\infty} = 1010 \pm 0.5$  for all silicate melts (and glasses) at  $\sim 20$ -1600 °C, which extends beyond the temperature range of most (contemporaneous) volcanic systems reported in the literature. Hence, the “temperature range of interest” is all volcanic temperatures.

Line 101: it might be useful to provide the equation for Ca here. - The paragraph details our knowledge of complex lavas (such as dome lavas) containing crystals and bubbles. The capillary number is highly relevant in aphyric lavas, but in the lavas discussed here, it remains to be adapted, which is beyond the scope of this study. Hence, we wish not to introduce the equation here and believe a qualitative description is sufficient.

Lines 134-144, and elsewhere: the authors describe two inclusion models which they highlight may explain their data: the pore-emanating crack model of Sammis and Ashby, and the sliding wing crack model of Ashby and Sammis. However, the authors do not go on to employ either of these models subsequently. As I intimated previously, it seems something of a shame that there is not a more involved analysis of these data. Analytical solutions for both these models are provided by Zhu et al. 2010 JGR and Baud et al. 2014 IJRMS, respectively. Previous authors have utilised one or other in order to describe the failure behavior of volcanic materials or analogues, for example Zhu et al. 2011 JGR (for tuffs), Vasseur et al. 2013 GRL (sintered glass), Heap et al. 2014 JGR (andesite), Zhu et al. 2016 JGR (basalts). Moreover, Zhu et al. 2011 extend the analytical solution to a dual-porosity medium, and Zhu et al. 2016 combine both models so as to have a representative element volume comprised of an effective medium including a pore surrounded by many cracks. If Coats et al. were to interrogate

[Printer-friendly version](#)[Discussion paper](#)

their data in a similar manner, they may be able to glean valuable information about the governing microstructural elements in their samples contributing to failure (for example by contouring for different values of  $K_{IC}/\sqrt{[\pi r]}$ ). -We thank Dr Farquharson for his detailed comments. Indeed, we had previously investigated the comparison of our data with the pore and wing-crack models but had excluded it from the results based on the assumptions of parameters we had to make in fitting the wing crack model. However, as the reviewer asked for this data we felt it important to extend our analysis. The following has been added to the manuscript in section 1.3:

An analytical estimation of this model was derived by Zhu et al., (2010) to estimate the uniaxial compressive stress ( $\sigma$ ) of a sample, with an average pore radius ( $r$ ), as a function of its porosity ( $\varphi$ ) and the fracture toughness ( $K_{IC}$ ):  $\sigma=(1.325)/\varphi^{0.414} K_{IC}/\sqrt{\pi r}$ , (2) The analytical approximation for this model was developed by Baud et al., (2014):  $\sigma=(1.346)/\sqrt{(1+\mu^2-\mu)} K_{IC}/\sqrt{\pi c} D_0^{-0.256}$ , (3) where  $\mu$  is the friction coefficient of the crack,  $c$  is the half-length of a pre-existing crack, and  $D_0$  is an initial damage parameter (which takes into consideration the number of cracks per unit area and their angle with respect to the principal stress). And the following in section 4.1.2:

The uniaxial compressive strength was calculated for the samples for both the pore-emanating crack model of Sammis & Ashby (1986) (Eq. 3) and the sliding wing crack model of Ashby & Sammis (1990) (Eq. 4). For the former, the uniaxial compressive strength was calculated with varying values of  $K_{IC}/\sqrt{\pi r}$  from 5 MPa to 25 MPa (Fig. 11). For the latter, approximate values for  $\mu, K_{IC}/\sqrt{\pi c}$  and  $D_0$  were taken from Table 3 in Paterson and Wong (2005) as 0.51, 20–30 MPa and 0.3–44, respectively. This gave a range of estimated strength between 54 and 90 MPa (Fig. 11). At higher porosities,  $> 0.25$ , the pore-emanating crack model with  $K_{IC}/\sqrt{\pi r} = 5\text{--}10$  MPa seems to fit the data well, whereas for most rocks with porosities of 0.12–0.2  $K_{IC}/\sqrt{\pi r} = 10\text{--}15$  MPa is a better fit. This could be explained by a decrease in the pore radius at these porosities, leading to higher values of  $K_{IC}/\sqrt{\pi r}$ , though, as the samples are heterogeneous and pore radius variability is high we cannot observe this (Figure 3). For the densest rocks

[Printer-friendly version](#)
[Discussion paper](#)


in the study ( $\sim 0.08\text{--}0.12$ ), the UCS data would suggest yet a higher  $K_{IC}/\sqrt{\pi r}$  of 20–25 MPa. The pore–emanating crack model could explain this switch in behaviour if there was a fundamental change in pore radius. However, the switch could also be explained by a transition in failure mechanism from pore–emanating cracks to wing cracks, meaning the wing–crack model would be more applicable. Alternatively, it may be a complex combination of the two. Although the solutions to the sliding wing–crack model are non–unique, as there are few experimentally constrained parameters, when combined with information gained from the pore structures (Fig. 3), the results of the modelling presented (Fig. 11) give us an insight into the dominant micromechanical failure mode of our samples. It is likely that the complex pore structures of these lavas, generated by a combination of vesiculation, deformation, and cooling-driven contraction require an as-yet undefined combination of the two models. The weighting towards one or the other, however indicates that for the higher porosity specimens the behaviour of failure could be described using the pore–emanating crack model of Sammis & Ashby (1986), whereas, in the lower porosity samples deformed in uniaxial compression, the main failure mechanism is explained by the sliding wing–crack model of Ashby & Sammis (1990).

Line 146: the authors should state clearly that they here define "lava" as something at high temperature (volcanic rocks may often also be referred to as lava). -We thank the reviewer for this comment and agree the definition between cold lava and high temperature lava was unclear at certain points in the manuscript. We have edited the manuscript with the following note: '[note: From here, samples deformed at high temperature will be defined as lavas, and those tested at room temperature as rocks].'

Line 184: in which direction has the lobe moved (i.e. rotation, inflation, advance)? - We have now added that: The mechanism of movement is thought to be down-slope advancement to the East (Matsushima and Takagi, 2000).

Line 279, and elsewhere: is this a change of 1 % or 1 vol.%? -It is a change of 1 vol.%. We have changed the manuscript to read 0.01 in place of 1%, in line with the method of

[Printer-friendly version](#)[Discussion paper](#)

reporting porosity used throughout the manuscript (e.g. Table 1). We have also noted this change elsewhere in the manuscript so that porosities are reported as a fraction. Where crystals are concerned we have reported these as vol.%

Line 296 and 298: which software was used to run the scripts? Are they publicly available? -The software used to run the scripts was MATLAB. A version of the script is now freely available on Github (<https://doi.org/10.5281/zenodo.1287237>). This has now been made clear in the manuscript.

Line 322: the observation that in dense materials the connectivity is higher than in porous materials is somewhat counter-intuitive, and runs counter to results from previous researchers (Farquharson et al. 2015 JVGR and Collombier et al. 2017 EPSL, both of which noted that connectivity generally increased with increasing porosity). Do the authors have any comment on this difference? -We agree it seems counter-intuitive, but the difference is very small: a matter of 0.01-0.02 unconnected pores. We attribute this to the presence of more small, isolated pores in the high porosity samples than in the low porosity samples. We also note that the porosity range of our rocks is considerably smaller (0.09-0.32) than Farquharson et al., (2015) (0.025-0.73) and Collombier et al., (2017) (~0.0-1.0), and so note that we are not evaluating the same range as these other studies. Our 'high porosity' samples could be considered low porosity in comparison to these other studies and so a comparison cannot be clearly drawn.

Line 342: cristobalite isn't a polymorph of quartz. Rather, both quartz and cristobalite are silica polymorphs. -We thank the reviewer for bringing this to our attention and agree the text would be clearer if the polymorph was referred to as a silica polymorph. The manuscript and Figure 3 have been edited in accordance with this.

Line 355-359: did sample volume change upon heating? This really is surprising, as one would anticipate thermal cracking upon heating and subsequent cooling, due to thermal expansion mismatch between the constituent microstructural components (e.g. Browning et al. 2016 GRL). This may be especially pronounced given the exis-

[Printer-friendly version](#)[Discussion paper](#)

tence of cristobalite in your samples, which undergoes a significant volumetric change as it transitions between its alpha and beta forms (a function of temperature: see for example, Damby et al. 2014 JAC). - We refer Dr Farquharson to the supplementary data, S5. Thermo-mechanical analysis (TMA) of the Mt. Unzen dome rock shows thermal expansion upon heating until the softening point of the material. We also refer him to lines 503-506 in the original manuscript (“A recent study by Eggertsson et al., in review, found that the strength and porosity of samples that hosted microfractures (like Mt. Unzen dome rock) were not affected by thermal stressing, while those that showed a trivial fraction of pre-existing micro-fractures were more significantly influenced through thermal stressing and as a result became more permeable.”). In accordance with Eggertsson et al., (2018), as our samples contained a pre-existing network of microfractures they were not readily fractured by thermal expansion and contraction. We also would like to point out that samples containing cristobalite, UNZ-13 (see Figure 3), were not tested at high temperature nor thermally stressed to avoid adding effects of mineralogical reactions in this study that would not be relevant in the lava dome setting – i.e. the cristobalite post-dates high-temperature emplacement. We also would like to state that the heating and cooling rates used ( $4\text{ }^{\circ}\text{C}\cdot\text{min}^{-1}$ ) were low enough to limit the differential expansion of the samples (that is, caused by temperature gradients across the samples, which also contribute to thermal cracking and which are not always considered independently from differential expansion of the constituent phases).

Line 378-380: it is not immediately clear from the figure, but does the rock stiffness increase with thermal stressing? Here you identify microfractures as the culprit, yet previously you indicate that thermal stressing doesn't affect the porosity of the samples. Moreover, I would think that induced cracking would serve to decrease the material stiffness, rather than increase it. I suggest the authors re-word this section for clarity and consistency. - No, the rock stiffness (i.e. Young's Modulus) does not increase with thermal stressing, it in fact decreases (Figure 9c and lines 479-498, original manuscript). We attribute the initial convex portion of the stress-strain curves to the closure of micro-

[Printer-friendly version](#)[Discussion paper](#)

cracks perpendicular and sub-parallel to the principal stress (as in Heap et al., 2014, JGR). This initial section of the stress-strain curve is more pronounced in the case of the thermally stressed samples (Figure 4c), indicating that either 1) the width of pre-existing macro-fractures increased or that 2) more microfractures (generated by thermal stressing) are available to close; however, the porosity determined from post-thermal stressing pycnometric measurements suggests that no micro-fracturing took place. We suggest that thermal stressing did indeed slightly modify the network of micro-fractures but on too-small a scale to affect the UCS and pycnometry results. The manuscript has been edited to highlight this observation and changes have been made to section 3.2.1.

Line 400-401: as previously, it would be useful if the authors were to distinguish between % and vol. %. - We have amended this throughout, as previously mentioned.

Line 431: Young's modulus ought to be capitalised. Also, there is a full stop missing at the end of this sentence. -These typos have now been corrected in the manuscript.

Line 441-445: see comment above concerning these inclusion models. -We have added analysis of these micromechanical models; see reply to comments above.

Line 470: could this observation be due to pore anisotropy (e.g. Bubeck et al. 2017; Griffiths et al. 2017)? - Here the reviewer is referring to the statement "This suggests that these samples are stiffer than the other specimens tested, and indeed those experiments reached unusually high peak stresses at relatively low strains to failure.", which is discussing samples UNZ-2 and UNZ-13. We looked at the thin section of UNZ-13 and conclude that the pore anisotropy may indeed contribute. Here the pores are preferentially aligned toward the principal stress direction (Fig.3) and so this is a likely case for stiffening. The manuscript has been amended at this line and in the conclusions section, see the reviewer's comment below. For UNZ-2 it is possible that these vesicles had a pore anisotropy that could have led to minor strengthening and an increase in stiffness, like that seen by Bubeck et al. (2017) and Griffiths et al. (2017).

[Printer-friendly version](#)[Discussion paper](#)

Yet, our investigation was not sufficient to constrain and explicitly state this as fact.

Line 480-481: do the authors have any information on the pore size distribution or pore anisotropy that could help explain this? -The reviewer is referring to the following statement “In addition, thermally stressed samples have slightly lower ( $\sim 0.5\text{--}1.5$  GPa) Young’s Moduli than their unstressed equivalents, as previously noted in dacites from Mt. St. Helens (Kendrick et al., 2013a). This highlights a potential change in porosity distribution that was not recognised by other means (e.g. total porosity, strength).”

The decrease in Young’s Modulus is very slight, therefore information on pore size distribution or pore anisotropy, e.g. from a thin section, is unlikely to help in explaining this decrease. As the samples are very heterogenous any change in pore behaviour would be difficult to quantify as the change would be expected to be small and comparing the exact material before and after thermal stressing is not possible in thin section. This would rely on pre and post stressing CT scans which are time consuming and would likely provided reconstruction with spatial resolution too low to accurately distinguish slight pore morphology changes. Hence, the most sensitive measure of change we have is the pycnometry – which as stated previously, did not indicate any change – and the mechanical data which shows a decrease in Young’s modulus.

Line 525: shear-induced development of pore connectivity was also shown experimentally by Kushnir et al. 2017 EPSL. -We regret the oversight in not citing this article and have now added it to the manuscript.

Line 535-560: as with my previous comments concerning the inclusion models of Ashby and Sammis and Sammis and Ashby, I believe the authors could extend this Deborah number analysis some more. As far as I can tell, the dimensions of Equation 10 only balance out if  $b = 1$ .  $Pa = [Pa \cdot s \times s^{-1}]$  is fine ( $b = 1$ ), but  $Pa = \sqrt{[Pa \cdot s \times s^{-1}]}$  is not, as would be the case were  $b = 0.5$ . To me, this highlights a serious shortcoming in the empirical approach adopted here, especially as there has been more recent work on the topic which adopt physical rather than empirical parameters, for example the

[Printer-friendly version](#)[Discussion paper](#)

Wadsworth et al. 2017 chapter referenced elsewhere in the manuscript. For example, that chapter addresses the physical scaling of  $De$  with crystal content. Ultimately, a similar physical approach could yield a much more generally applicable failure criterion for porous materials. -With regards to the units of Equation 11, the equation balances if constant  $k$  has units of  $\text{MPa}\cdot\text{s}^{1/2}$ , as shown below:  $\sigma(\text{MPa})=k(\dot{\epsilon} \text{MPa}\cdot\text{s})^{1/2} \dot{\epsilon} \text{MPa}\cdot\text{s}^{1/2}$

In the Wadsworth et al. 2017 chapter, only the single or two-phase cases are discussed. Within this chapter, the equation for the Deborah number is only given for a two-phase, crystal-bearing medium (Equation 3, Wadsworth et al., 2017). Here we are working with a three-phase medium, for which no models exist and thus an empirical approach must be adopted. For the sake of this argument, if we assume that the material from Mt. Unzen is a two-phase, crystal-bearing medium we can use Figure 2 in Wadsworth et al., (2017) to calculate the critical Deborah number expected. Given that the Unzen material has a crystal content,  $\dot{\epsilon}_x$ , (microlites+phenocrysts) of  $\sim 0.75$  we can use this to find the critical Deborah number if no bubbles were present. To find this critical value, the maximum packing fraction,  $\dot{\epsilon}_m$ , also has to be known. As  $\dot{\epsilon}_m$  is defined as “the volume fraction of particles beyond which there is no space remaining which would accommodate further particles” (Mader et., 2013), it is clear from thin section and SEM images that our material has not yet reached  $\dot{\epsilon}_m$  (see Fig. 3). Therefore, it can be assumed that for the Mt. Unzen material investigated here,  $\dot{\epsilon}_m \approx 0.76-0.99$ , and  $(\dot{\epsilon}_x)/(\dot{\epsilon}_m) = 0.76-0.99$ . According to Figure 2 in Wadsworth et al. (2017), this range gives the range of critical Deborah number as  $9.9 \times 10^{-5}-7.6 \times 10^{-4}$ . Therefore, our estimation of the critical Deborah number of the dense material as  $9.4 \times 10^{-5}-6.6 \times 10^{-4}$  is a very reasonable one indeed. The method used in this manuscript to find the Deborah number and then critical Deborah numbers is empirical but, as well as giving a working solution to find the Deborah number for a three-phase material, it shows that there is a reduction in critical Deborah number due to the addition of particles and also provides a linear relationship for the critical Deborah number and the addition of pores. This study is a novel, first-step approach into characterising the  $De$  number and failure

[Printer-friendly version](#)
[Discussion paper](#)


constraints on real, volcanic samples using mechanical testing data.

Line 535: using exp as a subscript is a little ambiguous (at first glance I presumed it signified an exponential). -For clarity, we have changed the exp subscript to obs to stand for observation in line with the symbol for observation time  $t_{obs}$ .

Line 546: Oswald should presumably be Ostwald. -Yes, this has now be changed in the manuscript.

Line 546: here, the authors state values of  $k$  and  $b$  of 1653 and 0.5, yet in the caption for Figure 10, the values are  $k = 1606$  and  $b = 0.7755$ . Which of these are correct? What is the sensitivity of the the following analysis to variations on  $k$  and/ or  $b$ ? -We thank the reviewer for pointing out this typo. The correct  $k$  and  $b$  values were those written within the manuscript. These values shifted due to an addition of data to the plot. We have now added the standard error of estimate for these values to the plot to show the variation of  $k$  and  $b$ .

Equation 11: Based on equation 9, shouldn't  $\sigma$  relate to strain rate  $\times$  viscosity (or equivalently,  $De \times G_{\infty}$ )? -We believe the reviewers confusion lies with the presentation of the equations, Equation 8 has now been edited from:  $De = \eta_m / (G_{\infty} t_{obs})$  to:  $De = \eta_m / (G_{\infty} t_{obs})$  (now Equation 9) And Equation 9 from:  $De = \epsilon \dot{\gamma}_{obs} \eta_m / G_{\infty}$  to:  $De = (\epsilon \dot{\gamma}_{obs} \eta_m) / G_{\infty}$  (now Equation 10) To get to Equation 11 from Equation 9 a substitution is made for  $\epsilon \dot{\gamma}_{obs}$ , which from Equation 10 is  $\dot{\gamma}_{obs} = (\sigma/k) \dot{\gamma}_{obs}^{1/b}$ . (now Equation 11)

Line 618: this is in contrast to existing theory, models, and experimental data. Perhaps this effect is masked in your data by sample heterogeneity? I would be wary of including this point as a key conclusion of the study. -The reviewer is referring to conclusion 3: The orientation of a vesicle may not necessarily have a discerning control on the strength of a rock, however it does have an influence on the strains reached at failure and, as such, the Young's Modulus. Here we agree with the reviewer and this point has now been removed as a key conclusion, in light of the discussion regarding

Printer-friendly version

Discussion paper



anisotropy in the reply to an earlier reviewer comment above made regarding line 470. The manuscript has also been edited to reflect this change.

Figure 4: there appears to be some data obscured by the legend in panels a and b. -We thank the reviewer for his keen eye and have clarified the figure accordingly.

Figure 6: for clarity, perhaps the authors could plot viscosity as a function of strain rate (similar to Figure 10a; perhaps with symbols coloured for time). -As the stress (which is proportional to viscosity) is plotted against strain rate on Figure 12b (previously Figure 10a). The b-value obtained from the curve in Fig 12b is 0.5 which matched the values obtained from previous studies on crystalline dome material (Caricchi et al., 2007; Lavallée et al., 2007, 2012), therefore we feel that there is no more information to be gained by alternative plots.

Figure 10: in panel a, the authors state that the equation is shown on the figure, but it is missing. In panel b (and line 555), is the relation given by the yellow line based on only three data (i.e. the transitional data)? What is the  $r^2$  value of this relation? Can the authors comment on the theoretical value of  $De_c$  for a nonporous material? Would this fit on the trend? Likewise, how do the authors anticipate  $De_c$  evolving for highly porous materials? -We thank the reviewer for highlighting this point which has spurred a number of changes (also in light of reviewer 2's comments). We now refer the reviewer to the revised Figure 12 and additional manuscript changes which have been edited to show two separate transitional regimes: viscous-dominated and brittle-dominated. Figure 12 shows clearly the evolution of failure and at which critical Deborah numbers this occurs. Figure 12c shows the standard error of estimate windows of this data and their  $R^2$  values. For a non-porous material, the data suggest the Critical Deborah number would lie between  $Dec = 1 \times 10^{-4}$  -  $6.6 \times 10^{-4}$ . This is approximately two orders of magnitude lower than that reported by Webb and Dingwell (1989), which we attribute to the high crystal content as crystals also decrease this critical Deborah number (Cordonnier et al., 2012; Wadsworth et al., 2017), see also the reply to reviewer's comments on lines 535-560 of the manuscript. For the porosity

Interactive  
comment

Printer-friendly version

Discussion paper



range of material tested herein, we expect the critical Deborah number to follow a linear trend as shown in Figure 12c.

Please also note the supplement to this comment:

<https://www.solid-earth-discuss.net/se-2018-19/se-2018-19-AC1-supplement.pdf>

Interactive comment on Solid Earth Discuss., <https://doi.org/10.5194/se-2018-19>, 2018.

SED

Interactive  
comment

Printer-friendly version

Discussion paper



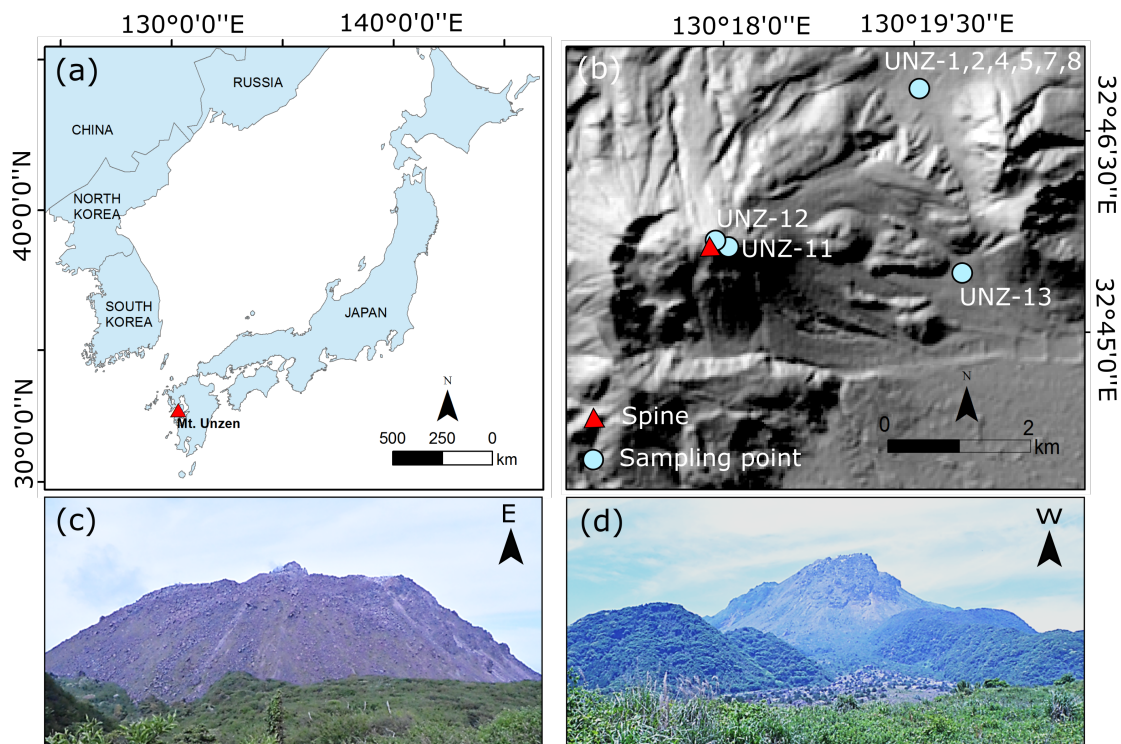


**Fig. 1.** (a) Location of Mt. Unzen in South Western Japan; (b) Sample collection locations and location of the erupted spine, the summit of Mt. Unzen at 1500 m above sea level (NASA/METI/AIST/Japan Spacesystem)

[Printer-friendly version](#)[Discussion paper](#)

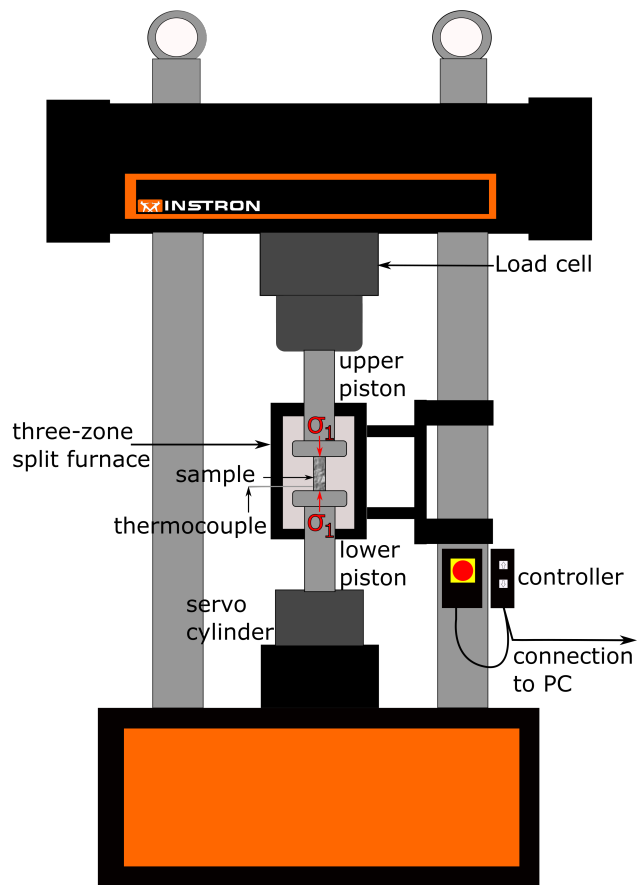


**Fig. 2.** Schematic of the uniaxial compressive strength testing set-up in the Experimental Volcanology and Geothermal Research Laboratory at the University of Liverpool. A 100 kN Instron 8862 uniaxial press

[Printer-friendly version](#)[Discussion paper](#)

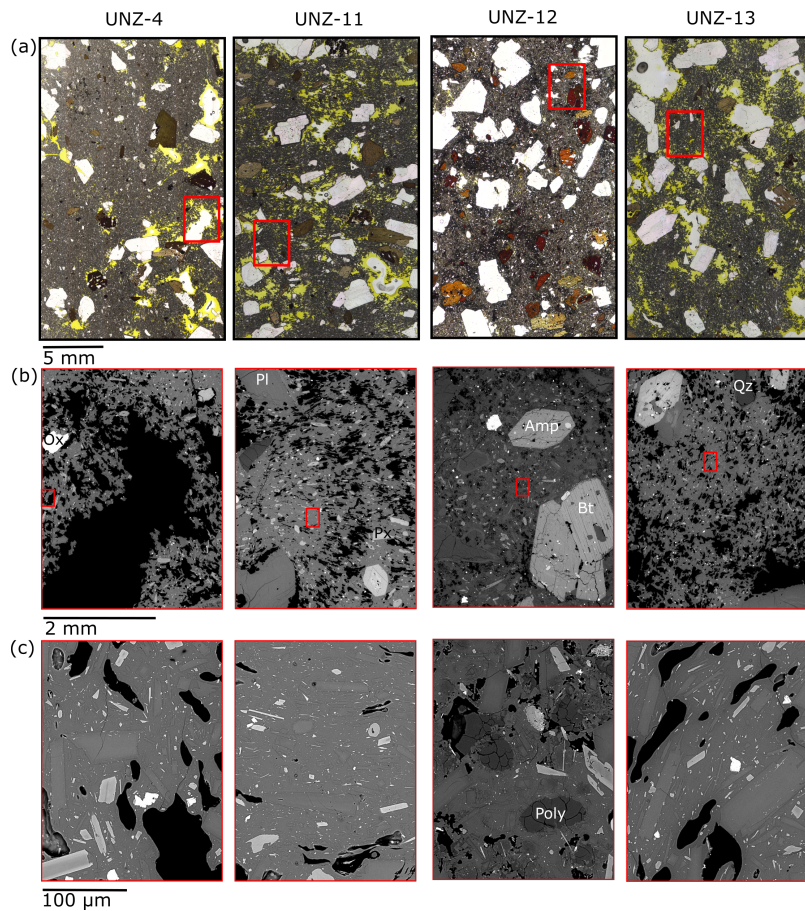


**Fig. 3.** Plane-polarised light (a) and backscattered electron images (b,c) of undeformed samples UNZ-4,-11, -12 and -13. (b) is a zoom into the red box in (a), and (c) is a zoom in of the red box in

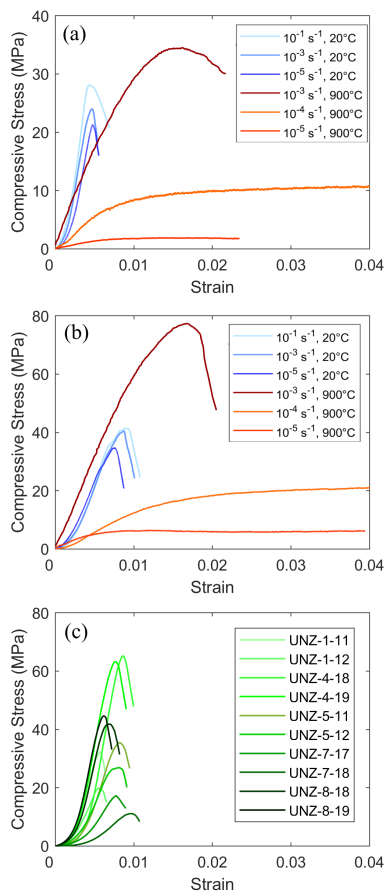


**Fig. 4.** Examples of compressive stress—strain curves for (a) high porosity, UNZ-1 (0.21); (b) low porosity, UNZ-4 (0.12) at a range of rates and temperatures and (c) thermally stressed samples, all

[Printer-friendly version](#)[Discussion paper](#)

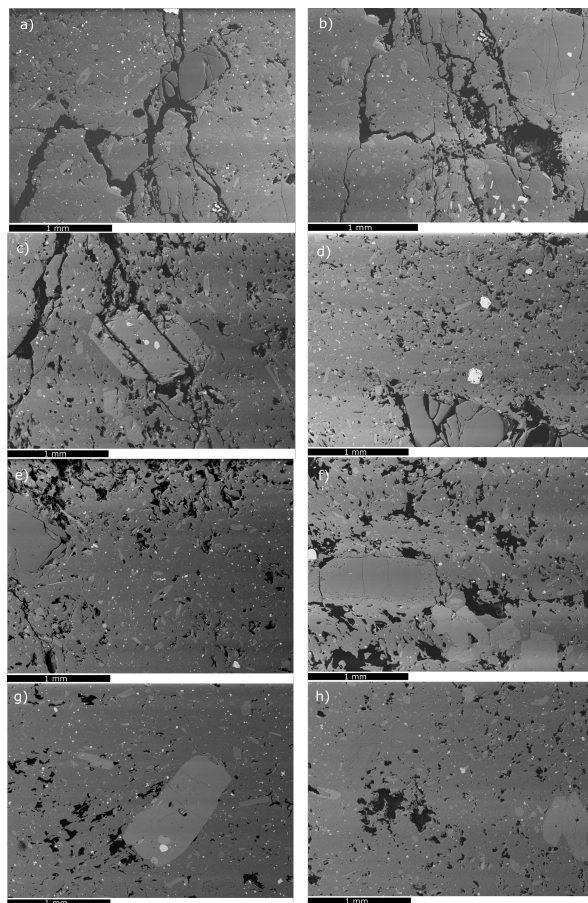


**Fig. 5.** Backscattered electron images of polished stubs for samples after strain a) to f) and before strain g) to h) (these are complimentary to Figure 11). Panels a), b) show sample UNZ-4-14 after

Printer-friendly version

Discussion paper



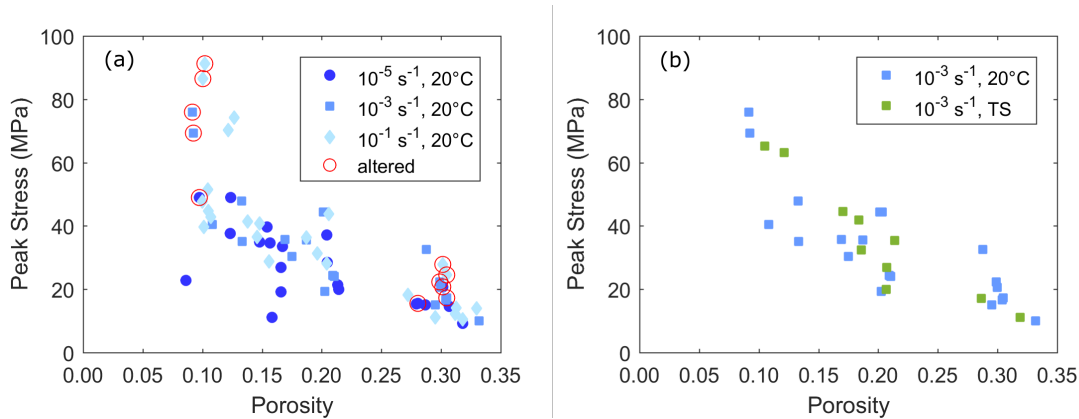


**Fig. 6.** (a) The strength (peak stress) of samples tested at ambient temperatures at varying strain rates, highlighting the apparent strengthening of materials deformed at faster rate. Red rings circle the sam

Printer-friendly version

Discussion paper



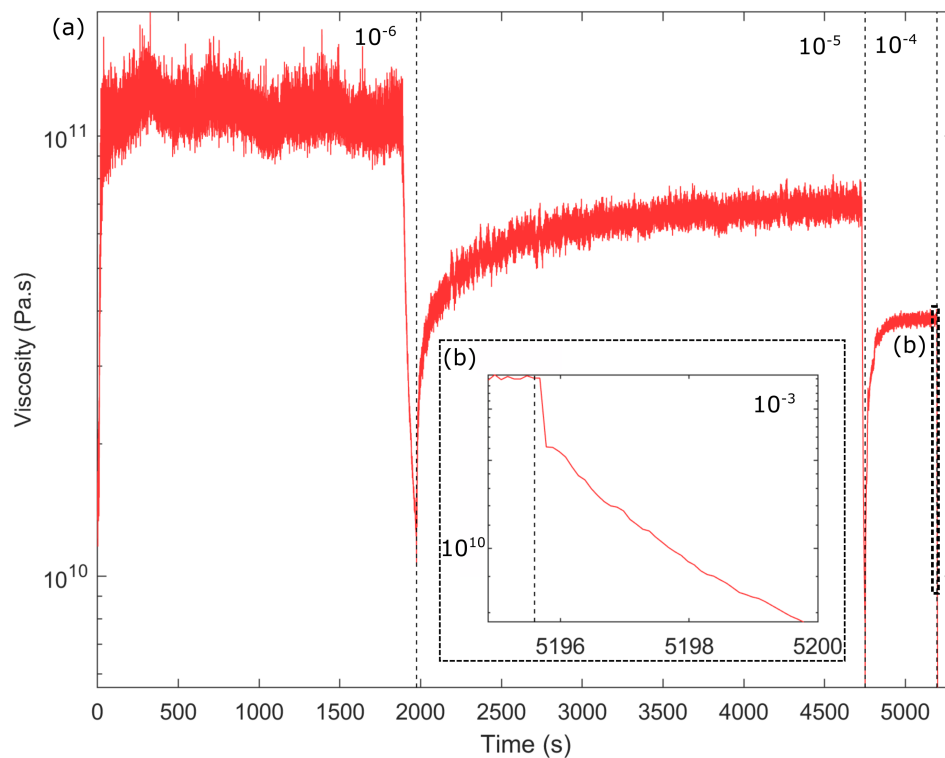


**Fig. 7.** Apparent viscosity evolution of UNZ-1 (porosity: 0.22) at 900 °C during a stepped strain-rate experiment ( $10^{-6}$  s $^{-1}$ ,  $10^{-5}$  s $^{-1}$ ,  $10^{-4}$  s $^{-1}$ ,  $10^{-3}$  s $^{-1}$ ); each step is separated by dashed lines. The insert z

[Printer-friendly version](#)[Discussion paper](#)

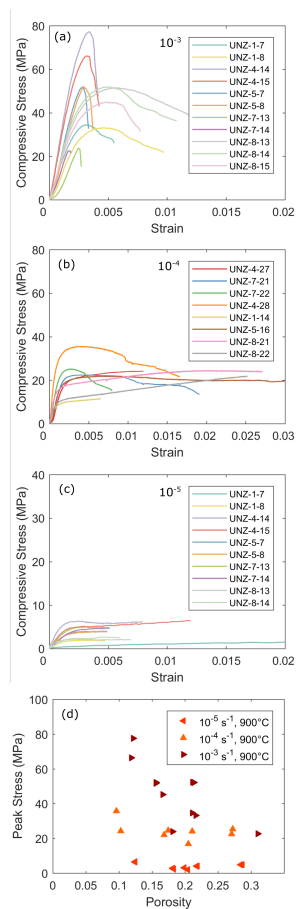


**Fig. 8.** High temperature uniaxial experiment results, including stress-strain curves for samples tested at a strain rates of (a)  $10^{-3} \text{ s}^{-1}$ , (b)  $10^{-4} \text{ s}^{-1}$ , and (c)  $10^{-5} \text{ s}^{-1}$ , demonstrating the shift from viscous

[Printer-friendly version](#)[Discussion paper](#)

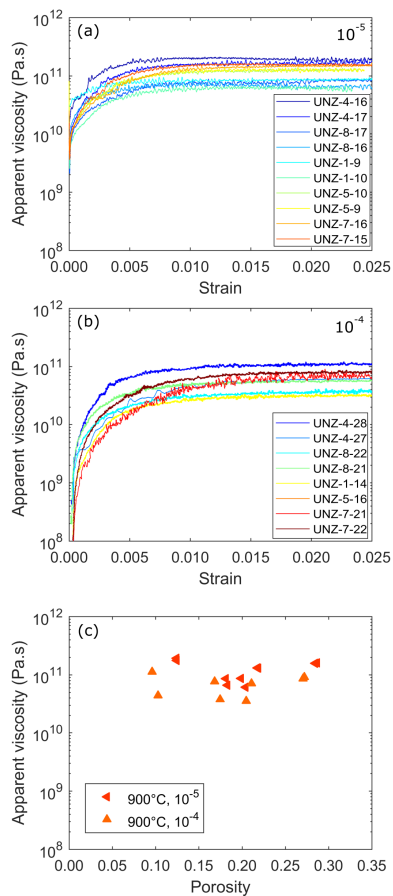


**Fig. 9.** Apparent viscosities of porous lavas at 900 °C for strain rates of (a)  $10^{-5}$  s $^{-1}$  and (b)  $10^{-4}$  s $^{-1}$ ; colours warm from blue to red with increasing sample porosity. (c) Compilation of apparent viscosities

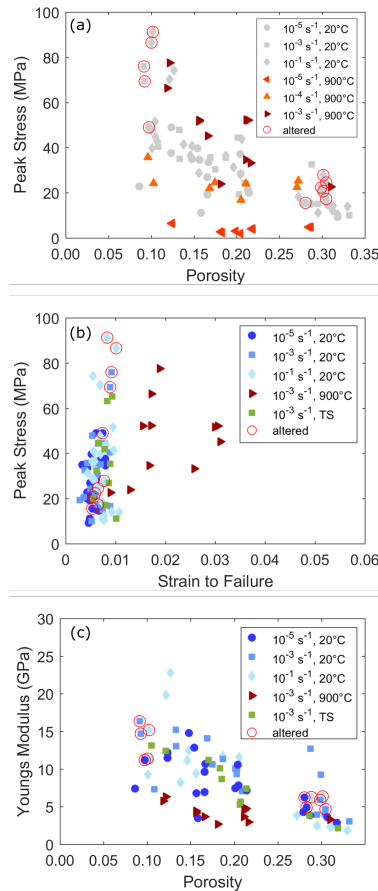


**Fig. 10.** Strength and Young's Moduli of Unzen rocks and lavas at different conditions. Shades of blue represent tests carried out at ambient temperatures, shades of red indicate those performed at 900 °C, and

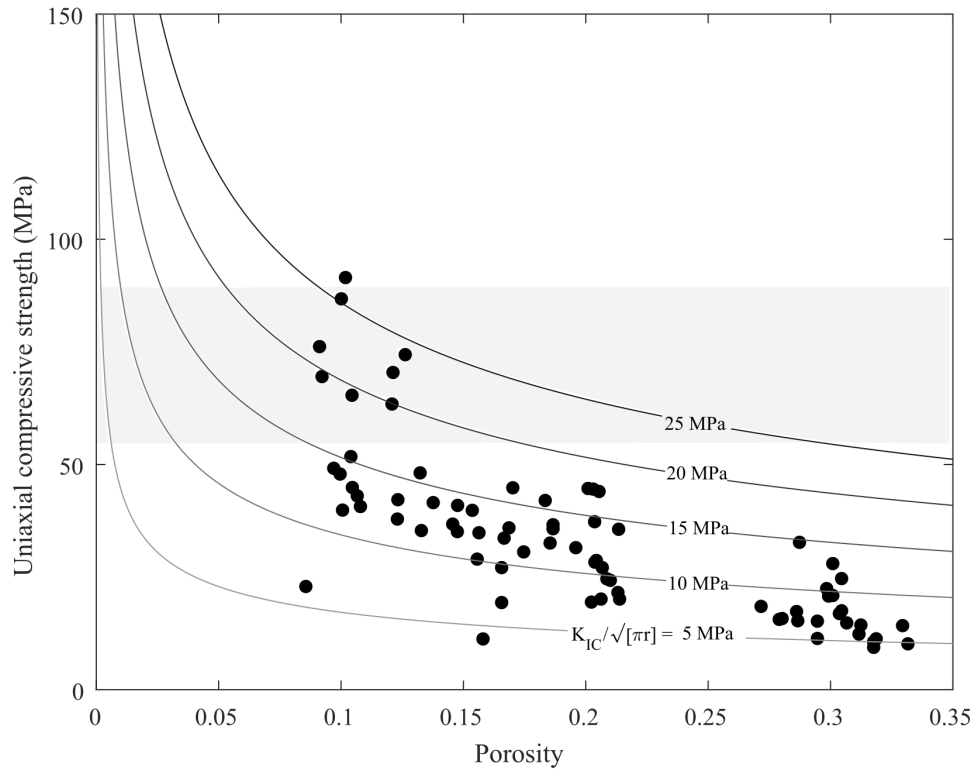


**Fig. 11.** The measured uniaxial compressive strength (UCS) for the samples (mechanical data) plotted against contours for various UCS calculated from the pore-emanaing crack model with different values (5–25 M

Printer-friendly version

Discussion paper



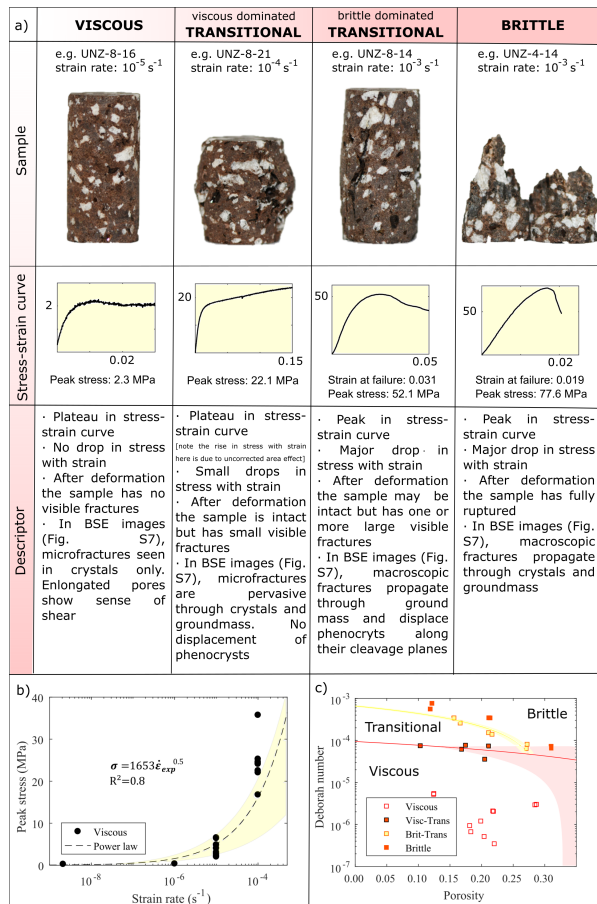


**Fig. 12.** (a) A schematic demonstration of sample rheological classification [viscous, viscous dominated transitional (visc-trans), brittle dominated transitional (brit-trans) or brittle], depending on the resp